Journal of Pharmaceutical Innovation (2020) 15:281–294
https://doi.org/10.1007/s12247-020-09438-0

ORIGINAL ARTICLE

Fast Continuous Non-Seeded Cooling Crystallization of Glycine in Slug Flow: Pure α-Form Crystals with Narrow Size Distribution

Mingyao Mou[1] · Mo Jiang[1]

Published online: 3 March 2020

Abstract

Purpose Glycine has been widely used as pharmaceutical excipients and synthesis reagents, and commercial glycine has a significant amount of aggregation and wide particle size distribution. A simple but reproducible process for generating uniform glycine crystals is always desired for both product quality and process efficiency purposes.

Methods Continuous cooling crystallization of glycine has been carried out in air-liquid slug flow in millimeter ID tubing, starting from solution without using seeds. Slugs were formed by combining air and liquid streams, then went through the crash cooling zone of varying lengths (tubing length in contact with ice bags). The operational boundaries of crash cooling times were evaluated: natural cooling (lower bound, no crash cooling), maximum cooling time for pure α-form without aggregation (upper bound), and beyond upper bound.

Results Non-aggregating pure α-form glycine crystals were continuously generated within ~ 10 min, feasible from multiple conditions (combinations of crashing cooling time and starting concentration). When crash cooling time further increases (while maintaining the starting concentration), crystal aggregations and/or γ-form crystals could appear. Reducing starting concentration can allow longer crash cooling time without widening product crystal size distribution or reducing crystalline form purity. At proper conditions, even natural cooling in slugs can nucleate and grow non-aggregated pure α-form crystals. All cooling conditions carried out in slug flow generally minimize needle-shaped crystals compared with corresponding batches.

Conclusion Glycine crystals of α-form and narrow size distribution can be continuously generated within 10 min from cooling crystallization in millimeter-sized slug flow, without using external seeds nor adding solvent/additives. And, the operational boundaries of crash cooling time (at proper starting concentrations) for pure α-form non-aggregating product crystals are identified.

Keywords Continuous crystallization · Glycine · Cooling nucleation · Slug flow · Aggregation · Polymorph

Introduction

During industrial development and manufacturing, most pharmaceutical molecules need to be processed into crystalline form for purification and/or formulation, due to the process robustness and low operational cost for crystallization [1–8]. The product quality consistency (e.g., dissolution rate and bioavailability) and manufacturing and process efficiency (e.g., blending and flowing) require the formation of uniform crystals of a specific form and controlled size/morphology [4, 5, 9–12]. For generating crystals, one simple approach is through cooling, whose strategies have been developed for continuous crystallizers, with high efficiency and reproducibility [13–15]. For stirred tank-based mixed suspension and mixed product removal (MSMPR) crystallizers [16, 17], liquid at target-desired temperatures is circulated through the crystallizer jackets. For pipe or tubular crystallizers (e.g., baffled crystallizers [15, 18], unbaffled crystallizers with mixing enhancer [19–21], laminar-flow crystallizers [7, 22–24], and segmented/slug-flow crystallizers [25–29]), cooling can be achieved through pipe/tube surface, such as pipe jackets

Electronic supplementary material The online version of this article (https://doi.org/10.1007/s12247-020-09438-0) contains supplementary material, which is available to authorized users.

✉ Mo Jiang
mjiang3@vcu.edu

Mingyao Mou
moum@vcu.edu

[1] Department of Chemical and Life Science Engineering, Virginia Commonwealth University, Richmond, VA 23219, USA

[30], merging in temperature-controlled zones such as water baths [25, 26], or natural cooling in air [25, 27]. While many continuous crystallizers such as MSMPR still operate with external/pre-made seeds, some tubular crystallizers can work on solutions directly through in-line nucleation [14], such as slug-flow crystallizer [14, 26, 31, 32].

Glycine has been used as pharmaceutical excipients in more than 170 drug formulations [33, 34]. Glycine is also widely used as a model compound for crystallization (together with solvent water) because of its well-studied solution and solid properties (solubility curve, polymorphism, etc.). The bulk pure glycine powder from commercial sources can be in crystalline form, but often includes significant aggregations and has a wide particle size distribution. Due to the large demands and various product applications of glycine powders (mostly in crystalline forms), simple but robust and reproducible methods for generating uniform glycine crystals are always needed. However, there are still challenges remaining for crystallization of glycine: (1) The temperature-sensitive solubility of glycine in water [35] allows using simple cooling for crystallization, and crash cooling was demonstrated in slug flow to nucleate and grow non-aggregated α-form glycine crystals from solution without using external seeds [25]. But, crystal uniformity (both form and size) can be very difficult to achieve from cooling alone. (2) The intrinsically fast growth rate of glycine crystals makes the control of narrow crystal size distribution more challenging [36, 37]. Specifically, sometimes, needle-shaped crystals are formed in such situations, which can significantly reduce process efficiency or even product quality [1–8, 38]. (3) Additional complexity from polymorphism of glycine crystals. Among their 3 common polymorphic forms (α, β, γ) at ambient temperatures, α-form is metastable but commonly available, and β-form is usually unstable, unless at certain conditions such as space confinement [34] or swift deep cooling [39]. The most stable γ-form is very difficult to generate from cooling in water alone, unless at relatively high starting concentrations and long residence time [40–42].

This article further explores the operational condition of crashing cooling in slug flow. Towards approaching the challenges, evidence is provided here answering these questions: (1) whether pure-form uniform-size (no needle-shaped crystals) glycine crystals can be generated in slug flow rapidly by non-seeded cooling crystallization alone (e.g., no antisolvent or additives—usually ending up with wide particle size distribution), and how is product crystal size distribution compared with batch experiments; (2) what is operational regime (and practical bounds for operational parameters, including cooling time and/or concentration) for uniform-form crystals without secondary nucleation nor aggregation; (3) whether γ-form crystals can be generated rapidly from cooling alone in aqueous slug flow without using additives.

Materials and Experimental Methods

Materials

Glycine was purchased from J.T. Baker (purity ≥ 99.5%), in α crystalline form (Fig. 1f). The solvent was deionized (DI) water. Prior to all crystallization experiments, saturated glycine solution was made and stored at corresponding solubility temperature, using the solubility expression of α-form below (for 5–60 °C) [35]:

$$C_{\mathrm{sat}}(T) = 0.563\, T_{\mathrm{sat\ exp}} + 9.836 \quad (1)$$

where C_{sat} (T) is equilibrium saturation concentration, g/100 g of water, and $T_{\mathrm{sat\ exp}}$ is experimental saturation temperature, in the unit of °C.

Cooling Crystallization in Slug Flow

As in Fig. 1a, slugs (for crystal nucleation and growth) were formed spontaneously by mixing hot glycine solution and air streams. A syringe pump (New Era syringe pump, model no. NE-4000) fed hot glycine solution from the heat-preserved syringe to the T-mixer point (polypropylene, ID = 3.125 mm), where the solution is segmented by another filtered air stream fed by a peristaltic pump (Masterflex L/S Precision Pump, Easy Load II Pump Head). The initial temperature, denoted as T_0, was the equilibrated temperature and maintained as the same in the syringe. The outlet of the T-mixer was connected to the 15-m tubular crystallizer (Masterflex, Platinum-Cured Silicon, L/S 16, ID = 3.125 mm). The first 10 cm of the tubular crystallizer was left in the air under room temperature (RT), and the following 0–1.6 m of the tubing was immersed in ice water bags (4 °C). All experimental conditions are detailed in Table 1, with 2 main variables (the starting concentration and crash cooling time), but we do not mean to cover all possible combinations. The crash cooling time was adjusted via changing the tubing length in direct contact with ice water bags. With different cooling times, the corresponding temperature profiles are different, as in Fig. 1c and d. For slug flow, the time profile refers to the same slug that goes through the length of the tubular crystallizer. The temperature was monitored with an IR laser thermometer to verify that every slug has the same temperature trajectory. Other parameters such as flow rate and residence time remain the same. The residence time is 10 min, at a linear flow rate of ca. 25 mm/s. The total

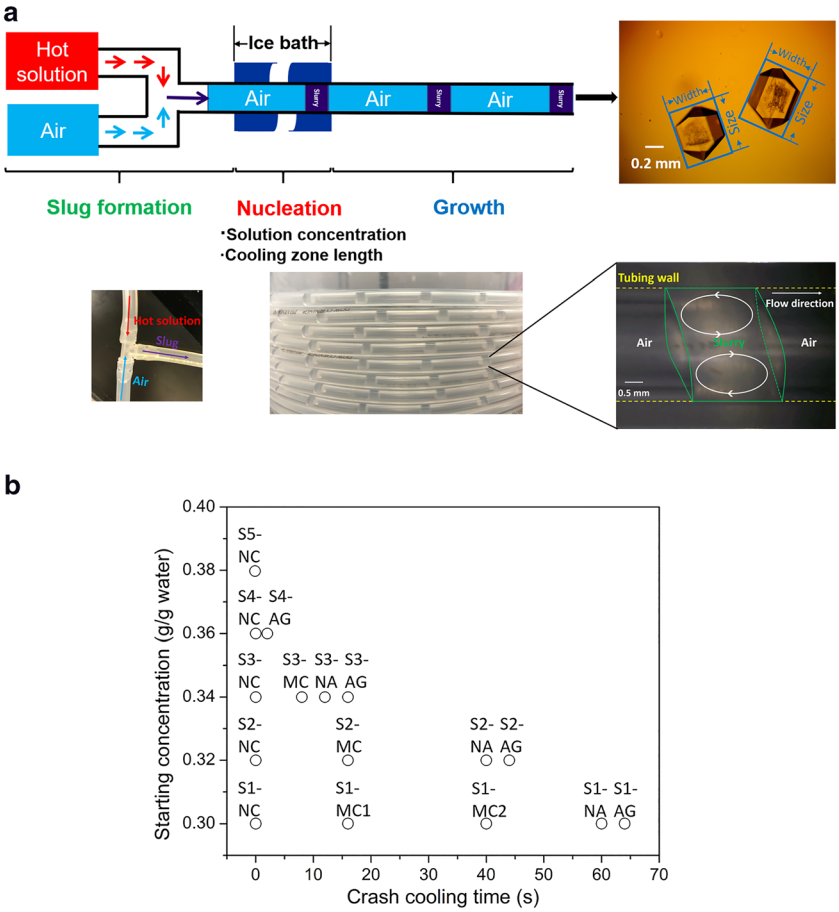

Fig. 1 **a** Scheme of the slug-flow crystallizer with decoupled subprocesses (including slug formation, nucleation, and growth and their related main considerations [14]) and photos of corresponding equipment below. A representative off-line microscope image (with polarizer) of product crystals in slugs (top right). In this work, the longest dimension of each crystal (e.g., aided by using an appropriate bounding box) is used for the size (major axis, or "length") of that crystal [43, 44], with width (perpendicular dimension to length on the image) also quantified. Snapshot of a representative slurry slug (containing crystals) separated by two slugs of air (lower right). The boundary of the slurry slug was indicated in the green line, and the inner tubing wall in yellow dash line [25]. **b** Experimental conditions (starting concentration and crash cooling time) for slug flow and batch crystallization experiments. Due to space limitations, only experimental number of slug-flow crystallization is labeled, and the corresponding batch crystallization experimental number is in Table 1c, d Representative time profiles of the temperature (blue) and corresponding relative supersaturation (orange) in SFC and batch crystallizers, under **c** crash cooling conditions (e.g., S2-NA with cooling time of 40 s) and **d** natural cooling (S2-NC) conditions. The relative supersaturation for the first 1 min was estimated, based on the measured temperature profile and solubility expression [35]. After 1 min, the assumption of negligible crystal mass is not likely to hold anymore, and supersaturation will be released (reduced) due to crystallization. **e** Microscope image and **f** XRD spectra of the commercial pure glycine powder, used as starting material (solute) for all crystallization experiments here

solution volume for each slug-flow crystallization is 10 mL. At the exit of the ice water bag region, the tubing sat in the air for the residual tubing length at RT (20 ± 2 °C).

Batch Cooling Crystallization

Corresponding batch crystallization of each SFC was performed for comparison, respectively. Using the batch experiment of B1-NA (counterpart of S1-NA) as an example, 3.0 g glycine was fully dissolved in 10 g water in a 10-mL conical Eppendorf tube (making the solution concentration 0.30 g glycine/g water as in Table 1) and kept at 40 °C initially. When the temperature reduced to 35 °C (the same temperature right before the nucleation region in SFC process), the mixture was poured into a shaken vessel with ice water wrapping (4 °C) for cooling time t in Table 1 (t = ice water bag length / linear flow rate). Then, the solution was poured back to its original vessel immediately and shaken. The time profile of the solution temperature (measured by IR thermometer) and supersaturation (calculated based on solution concentration and measured temperature) inside the batch are shown in Fig. 1c and d. For batch experiments, the time

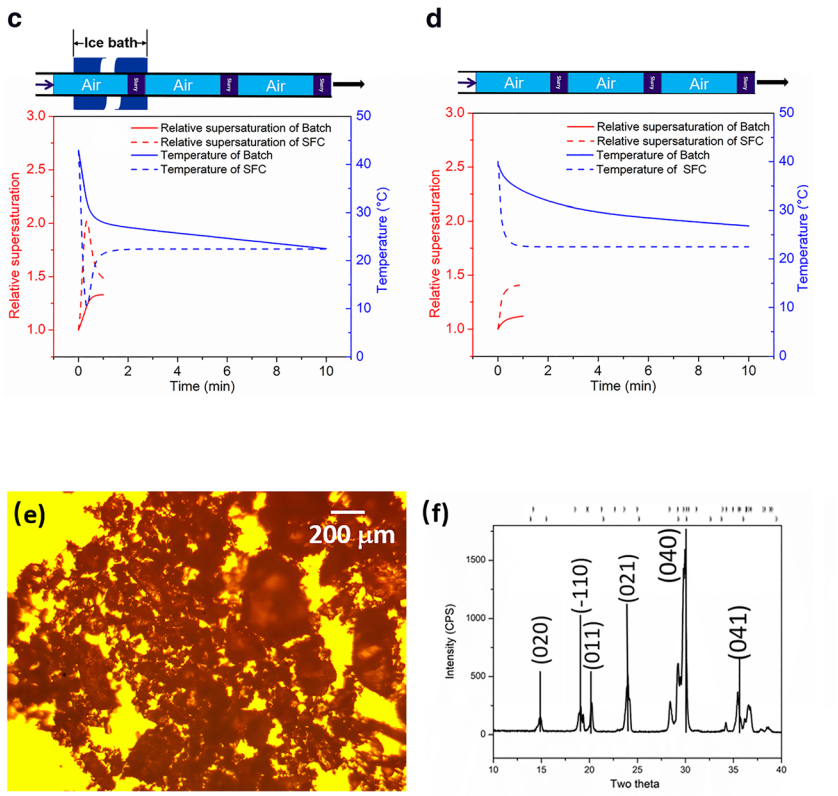

Fig. 1 (continued)

profile refers to the time evolvement of temperature in a set location within the batch (e.g., near the wall) due to heat transfer from the wall.

Crystal Characterization

For slug-flow experiments, all slugs are collected for quantifying size statistics. The product was collected in a 96-well plate with 2 slugs per well, followed by adding two droplets of mineral oil immediately to suppress evaporation. Off-line images for these slugs in wells (Fig. 2) were taken immediately after collecting the product, using Amscope ME520TA microscope equipped with an MU-900 camera. For batch experiments, after 10 min (same residence time as the SFC), one droplet of product slurry was collected from the upper and bottom part of the vessel each, then placed onto a glass slide and taken off-line images immediately. The rest of the batch experiments are deduced by analogy. The crystal size statistics (from analyzing off-line images using ImageJ) for slug-flow crystallization (SFC) and batch experiments are summarized in Tables 2 and 3, mainly for experiments without crystal aggregation. The crystal size info for each slug of all experiments is detailed in Figs. S1 and S2, and crystals can continue to grow in collection well plates if supersaturation had not been fully consumed during the short residence time (10 min) of slug flow (Fig. S3).

Then, the product slurry was centrifuged (with the supernatant discarded) before the crystals were dried in air overnight and stored for structure (solid form) and yield characterization. X-ray powder diffraction spectra (XRD, Rigaku, MiniFlex II, USA) were taken for glycine solids of product from all experiments and starting materials (Fig. 3). The solid forms were analyzed based on the XRD spectra, with form portion (Tables 2 and 3) estimated based on the total integrated area of all characteristic XRD peaks (Fig. 3a–d) as in literature [41, 45–47]. The pure α- and γ-form spectra (reference XRD spectra) are obtained from Crystallography Open Database (ID 7201582 and 2103307, respectively) [41, 45–47].

The actual yield (based on crystals collected by a certain time, e.g., 10 min, as in this article) and theoretical yield were calculated as follows:

$$\text{Actual yield} = \frac{\text{Dried crystal mass}}{\text{Total solute mass}} \times 100\% \quad (2)$$

$$\text{Theoretical yield} = \frac{(\text{Ci} - \text{Cs@RT}) * \text{Total solution mass}}{\text{Total solute mass}} \times 100\% \quad (3)$$

where *Ci* refers to the initial concentration (e.g., at elevated temperature), and Cs@RT refers to the solubility of glycine at room temperature.

Table 1 Different conditions of slug-flow crystallization (SFC) and batch crystallization. The total solution volume that is 10 mL for all conditions is the same. Corresponding batch experiment for each SFC process keeps the same residence time, initial temperature, and total volume. All conditions of slug flow have most experimental parameters the same such as the linear flow rate (25 mm/s), residence time (t_r, 10 min), and the slug aspect ratio (0.8), but vary in the initial temperature T_0, concentration (C), and cooling region length (l_{cool}), aka cooling time (t_{cool}). The maximum relative supersaturation ($S_{r,max}$) was calculated based on the temperature profile of SFC (e.g., Fig. 1c, d). As the α-form is the major crystalline form of glycine product crystals, the supersaturation estimation is based on the solubility of α-form glycine [35]. For the condition numbers in the table, "S" and "B" refers to slug-flow crystallization and batch crystallization, respectively. Numbers after S and B stands for different starting concentration. Abbreviations of natural cooling, medium cooling, aggregation, and non-aggregation data points are NC, MC, AG, and NA, respectively

SFC #	l_{cool} (m)	Corresponding batch no.	$C_{glycine}$ (g/g water)	T_0 (°C)	$S_{r,max}$	t_{cool} (s)
S1-NC	0	B1-NC	0.30	40	1.33	0
S1-MC1	0.4	B1-MC1	0.30	40	2.45	16
S1-MC2	1.0	B1-MC2	0.30	40	2.45	40
S1- NA	1.5	B1-NA	0.30	40	2.45	60
S1- AG	1.6	B1-AG	0.30	40	2.45	64
S2-NC	0	B2-NC	0.32	40	1.42	0
S2-MC	0.4	B2-MC	0.32	40	2.61	16
S2-NA	1.0	B2-NA	0.32	40	2.61	40
S2-AG	1.1	B2-AG	0.32	40	2.61	44
S3-NC	0	B3-NC	0.34	42.9	1.51	0
S3-MC	0.2	B3-MC	0.34	42.9	2.62	8
S3- NA	0.3	B3-NA	0.34	42.9	2.68	12
S3- AG	0.4	B3-AG	0.34	42.9	2.74	16
S4-NC	0	B4-NC	0.36	46.5	1.65	0
S4-AG	0.05	B4-AG	0.36	46.5	2.24	2
S5-NC	0	B5-NC	0.38	50.0	1.80	0

Result and Discussion

Fast Generation of Glycine Crystals with a Narrow Size Distribution from Cooling in Slug Flow

Within 10 min of cooling the glycine solution (no seeds used), the slug-flow cooling crystallization process under certain conditions (as detailed later) can already generate pure α-form crystals with narrow size distribution (Fig. 2), and without needle-shaped crystals nor aggregation. The glycine solution was made from dissolving glycine powder (starting material) in water, with the powder containing large amounts of aggregation and crystals of a wide size distribution (Fig. 1e, f). Effective factors for tuning product crystal size distribution from cooling crystallization are evaluated. As demonstrated with well-studied batch experiments [6, 8, 48, 49], the outcome of cooling crystallization can be improved by seeding [50], or controlling the supersaturation time profile (e.g., starting concentration, temperature range, and cooling rates) [4, 8]. For continuous cooling crystallization without pre-made seeds, key factors (discussed in the "Lower Bound of Crash Cooling Time: Natural Cooling" and "Upper Bound of Crash Cooling Time for Pure α-Form Without Aggregation" sections) include the starting concentration (the dominating factor well recognized [6, 8, 48, 49]) and temperature range (or temperature-time profiles, which can be adjusted with crash cooling time, as in Fig. 1c, d). For the same cooling crystallization conditions (residence time, cooling source), the product crystals from slug flow and batch crystallizers have very different sizes and even polymorphic form statistics. (1) For most conditions tested, product crystals from batches show at least two size populations (Figs. 2 and S2b), with the small-size population sometimes in needle shape (Figs. 5c and 2). The result is likely due to spatially non-uniform supersaturation, due to surface cooling. In comparison, product crystals from slug flow (Fig. 2) are larger in average size, but less variation, especially no needle-shaped crystals. Usually, situations with larger average size and fast growth are more difficult to maintain narrow size distribution. In addition, the slug-flow statistics are calculated using all nucleated slugs (~5–10 mL), which tends to widen the apparent size distribution due to possible crystal growth and nucleation while waiting in collection wells (Fig. S1d). If using similar sampling volume as batch, then, crystals from slug flow will have even much narrower size distribution. The reason is that the current sampling volume of slug flow is about 50 times larger than batch, and even double the current sampling

size of batch (e.g., from 2 droplets to 4 droplets) would evidently widen the size distribution, as indicated in Fig. S2b. The continued growth and possible nucleation of crystals inside collection wells are mainly due to remaining supersaturation after 10 min inside the tubing and can be reduced by increasing residence time (connecting current tubular crystallizer to longer tubular crystallizer), or accelerated growth using seeds at the beginning. These possible modifications are separate topics, not the focus of this article.

(2) At low starting concentrations and/or cooling time (e.g., S1-NC and S1-MC1 in Table 3 and Figs. 1b and 2), slug flow can nucleate crystals when batches fail to nucleate, likely due to the faster heat transfer in slug flow [14, 26, 31, 32, 51]. As nucleation in small volume is stochastic [25], the specific portion of slugs nucleated can be affected by experimental conditions, as quantified in Table 2. (3) As the starting concentration increases within a proper range (0.30 to 0.34 g/g), both the crystal average dimension (length and width) and short-term yield from slug flow increase (Tables 2 and 3 and Fig. 4), due to increased supersaturation (Fig. 1c, d) and higher theoretical yield (from mass balance), as discussed in the "Lower Bound of Crash Cooling Time: Natural Cooling" and "Upper Bound of Crash Cooling Time for Pure α-Form Without Aggregation" sections. Batches do not show such a clear trend of average crystal dimension with respect to the starting concentration, likely due to the existence of non-uniform supersaturation and uncontrolled secondary nucleation, as discussed in the previous paragraph. (4) Most product crystals are in α-form. Different polymorphic forms (α- and γ-forms) from two crystallizers are discussed in the "Beyond Upper Bounds: γ-Form Glycine Crystals Generated from Cooling Aqueous Slugs" section.

In this specific case where cooling was used for both nucleation and growth, the operational range of starting concentration covers 0.30 to 0.34 g glycine/g water, with corresponding crash cooling time in Fig. 1b. The operational range of starting concentration is almost always bounded. For example, overcooling (high supersaturation or long retention time under supersaturation) can result in too many nucleation and aggregation [4], while undercooling (low supersaturation or short retention time under supersaturation) can result in non-enough crystals or too long crystallization time. Thus, the lower bound of concentration shall still be enough supersaturation for primary nucleation, and the upper bound shall not be too high supersaturation for too much secondary nucleation nor tubing fouling or clogging. If needed for manufacturing purposes, the concentration range can certainly be extended with additional tools, such as finer control of nucleation [22, 24] and temperature profile along the whole crystallizer (tubing) length [28, 30, 52].

Fig. 2 Microscope images of batch sample and representative slurry slugs from cooling crystallization experiment, together with volume-based cumulative crystal size distributions from these samples (red curve for batch and black curve for slug flow), for **a** natural cooling (zero crash cooling time), **b** 16 s cooling time, **c** 0.30 g/g starting glycine concentration, and **d** 0.32 g/g starting glycine concentration. Scale bar, 200 μm. Experimental conditions and product crystal statistics are detailed in Tables 1, 2 and 3, respectively. For cumulative size distribution, both length-based and width-based distributions are included. For batch crystal images, samples are 2 droplets combined from the upper and lower location of the batch (using plastic pipettes). Representative images from individual droplets are in Fig. S2b. For slug crystal images, all slugs are sampled (e.g., 5–10 mL, or ~ 50 droplets), and each image is ~ 2 slugs (~ 1 droplet)

Lower Bound of Crash Cooling Time: Natural Cooling

Natural cooling usually reduces product quality [4] and causes operational difficulty (e.g., tubing blockage), thus not recommended for batch operations. The results here indicated that there may still be some use of natural cooling in slug flow. For example, at high starting concentration (e.g., 0.36 g/g water), natural cooling in slug flow can still generate well-separated crystals, when crystal aggregation would occur for the same starting concentration using crash cooling. At lower concentrations (e.g., 0.30 and 0.32 g/g water), almost no nucleation occurs in batch (Table 3, Fig. 2), while there is some nucleation from natural cooling in slug flow (Table 2, Fig. 2). Considering the much smaller volume for each slug (compared with batch) will lower the nucleation possibility, the higher nucleation rate from slugs (even with natural cooling) may come from the faster heat transfer rate in slugs due to recirculation, so that the slug volume is more effectively cooled from surface (Fig. 1c, d) than in batch. In other words, with a short period of cooling time with cooling through the surface, only part of the batch volume has enough supersaturation for nucleation. In addition, no secondary nucleation has been observed from natural cooling crystallization in slugs. In contrast, all batch experiments generate crystals with a large variation of coefficient, even at a small average size, indicating very different sizes (also confirmed in Fig. 2 showing at least an order of magnitude difference in size) and secondary nucleation. A possible reason is the spatially non-uniformity of temperature and supersaturation (Fig. 1c, d) [6, 48, 49, 53], which leads to spatially different nucleation and growth rates, and different residence time of crystals.

At the same starting condition, a higher *cooling rate* (heat transfer rate) can lead to higher supersaturation thus higher nucleation and growth rates ([4] [1–3]). From Table 2, the nucleated slug portion is always higher from crash cooling (NA) than from natural cooling (NC). And, the same trend occurs for batches based on the total number of crystals per sampling volume (Table 3). This trend and the difference in nucleation (nucleus number) are more evident at lower starting concentrations when the maximum supersaturation is lower, thus more difficult to nucleate. Slug-flow experiments using both natural cooling

a

Concentration (g/g water)	Batch	Slug	Q3-L-CSD	Q3-W-CSD
0.30	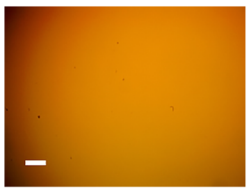		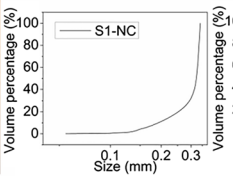	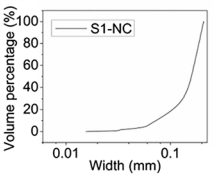
0.32	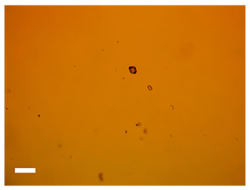		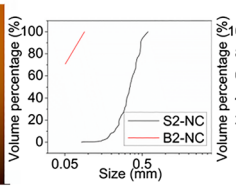	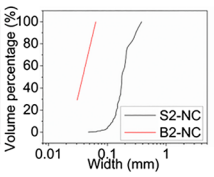
0.34	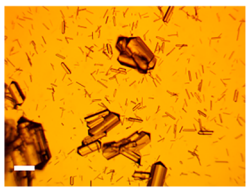	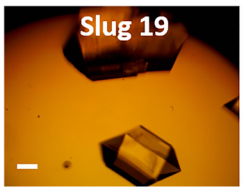	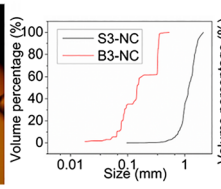	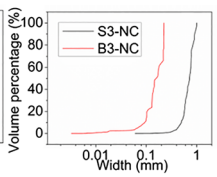
0.36	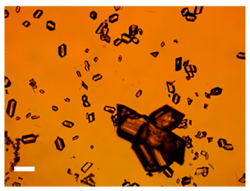		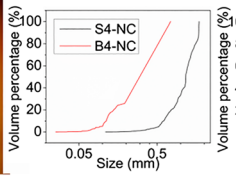	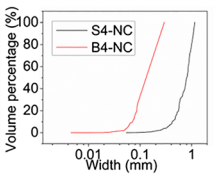

b

Concentration (g/g water)	Batch	Slug	Q3-L-CSD	Q3-W-CSD
0.30	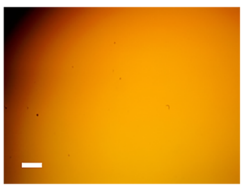	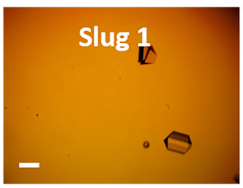	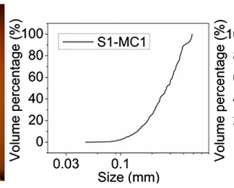	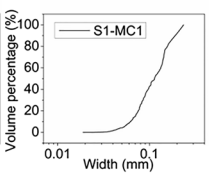
0.32	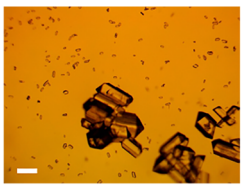		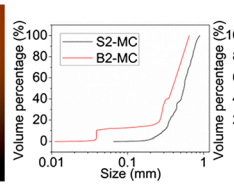	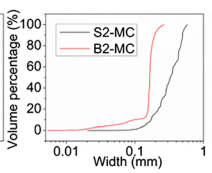
0.34	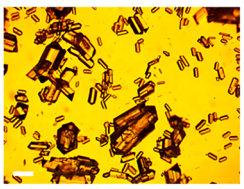	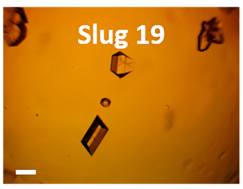	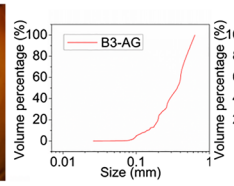	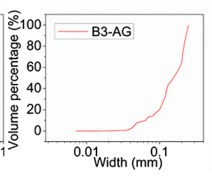

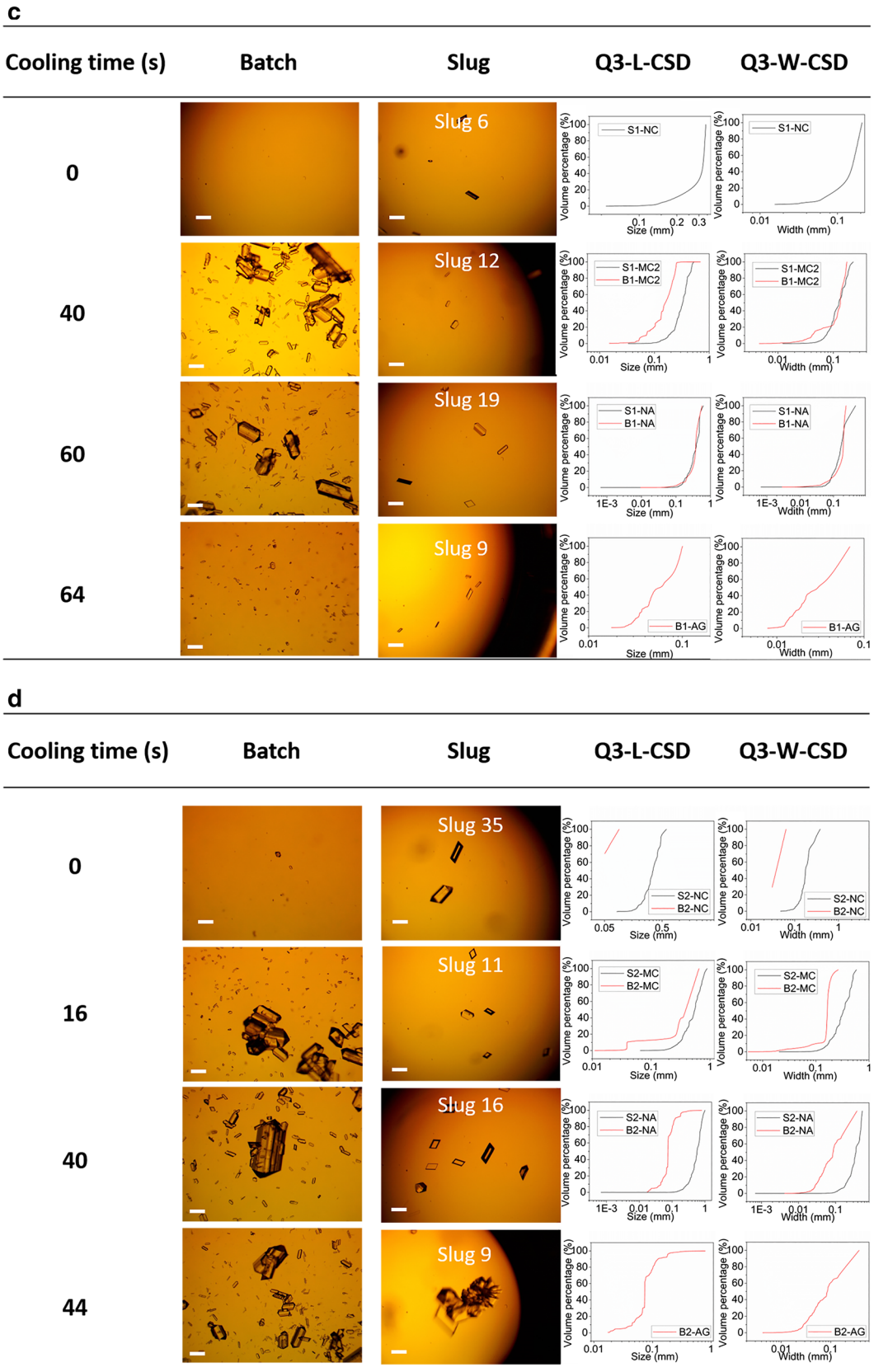

Fig. 2 (continued)

Table 2 Size statistics of pure α-form non-aggregated product crystals from slug-flow cooling crystallization experiments. Detailed conditions are in Table 1. The size statistics are analyzed for experiments with the outcome of pure-form crystals without aggregation, and other experiments (e.g., with aggregation) are also listed in the same table for comparison purposes. The sampling volume for size statistics is the total volume of all slugs nucleated, which is 1.5–10 mL. The real variation is lower than in Table 2 (apparent variation), due to contribution from crystal growth and nucleation in static collection wells with different measurement waiting time (Fig. S1d). "SD" for standard deviation, and "CV" for coefficient of variation, respectively. The 10-min yield is based on crystal mass collected immediately at the tubular crystallizer exit (after a residence time of 10 min). Long-term yield always approaches theoretical yield (based on temperature-solubility function as in Eq. 1), which are 29.7%, 34.1%, 38.0%, and 41.4% for starting concentrations of 0.30, 0.32, 0.34, and 0.36 g/g water, respectively. As with literature [41, 45–47], the polymorphic form portion (%) is approximated by the total integrated area of all characteristic XRD peaks for α-form and γ-form (Fig. 3). In another word, the total portion of α-form and γ-form is 100%

Condition number	Cooling length (m)	% of nucleated slugs	Total number of crystals, N	10-min yield (%)	Apparent mean length (mm)	Apparent SD, L (mm)	Apparent CV, L	Apparent mean width (mm)	Apparent SD, W (mm)	Apparent CV, W	~ % α-form
S1-NC	0	15	13	2.4	0.16	0.11	0.66	0.07	0.05	0.8	100
S1-MC1	0.4	89	299	17.8	0.28	0.16	0.55	0.09	0.06	0.7	100
S1-MC2	1	86	330	9.3	0.2	0.1	0.5	0.08	0.04	0.51	100
S1- NA	1.5	92	156	11	0.21	0.11	0.52	0.09	0.05	0.6	100
S1- AG	1.6	97	/	/	/	/	/	/	/	/	100
S2-NC	0	58	99	11.6	0.25	0.1	0.41	0.13	0.06	0.42	100
S2-MC	0.4	98	279	19.2	0.31	0.16	0.53	0.18	0.1	0.57	100
S2-NA	1	95	171	22.5	0.29	0.18	0.65	0.17	0.11	0.66	100
S2-AG	1.1	100	/	/	/	/	/	/	/	/	100
S3-NC	0	88	135	35.1	0.76	0.43	0.57	0.45	0.24	0.53	100
S3-MC	0.2	100	275	33.9	0.45	0.26	0.57	0.27	0.15	0.56	100
S3- NA	0.3	96	257	36.1	0.4	0.19	0.47	0.25	0.12	0.49	89
S3- AG	0.4	10	/	/	/	/	/	/	/	/	80
S4-NC	0	94	187	6.8	0.48	0.36	0.75	0.3	0.24	0.8	100
S4-AG	0.05	100	/	/	/	/	/	/	/	/	80

(NC) and crash cooling (NA) start with the same conditions (solution temperature, concentration) and end up at the same final temperature (room temperature). Compared with natural cooling, crash cooling usually has a faster initial cooling rate

Table 3 Size statistics of product crystals from batch experiments corresponding to slug-flow experiments in Table 2. Definitions of all parameters are the same as Table 2. The sampling volume is 70 μL (2 droplets), from upper and lower locations within the batch. Batches B1-NC and B1-MC1 did not nucleate; thus, no crystal data included

Condition number	Cooling time (s)	Total number of crystals, N	10-min yield (%)	Mean length (mm)	SD, L (mm)	CV, L	Mean width (mm)	SD, W (mm)	CV, W	~ % α-form
B1-NC	0	0	0	0	/	/	/	/	/	/
B1-MC1	0	0	0	0	/	/	/	/	/	/
B1-MC2	40	134	1	0.09	0.08	0.9	0.03	0.04	1.05	100
B1- NA	60	178	0.4	0.07	0.07	0.96	0.02	0.03	1.57	100
B1- AG	64	134	1.35	0.04	0.01	0.36	0.02	0.01	0.51	100
B2-NC	0	2	0	0.07	0.03	0.39	0.05	0.02	0.49	100
B2-MC	16	126	11.9	0.06	0.09	1.48	0.03	0.04	1.32	100
B2-NA	40	184	11.6	0.09	0.08	0.82	0.04	0.04	0.9	100
B2-AG	44	114	20.7	0.08	0.06	0.76	0.03	0.03	1.03	100
B3-NC	0	128	15.3	0.14	0.13	0.89	0.04	0.06	1.36	100
B3-MC	8	182	17.8	0.1	0.08	0.8	0.03	0.05	1.42	100
B3- NA	12	137	20.7	0.1	0.09	0.86	0.03	0.05	1.42	100
B3- AG	16	126	19.8	0.09	0.09	1	0.04	0.04	0.96	100
B4-NC	0	75	23.6	0.09	0.08	0.92	0.05	0.04	0.74	82
B4-AG	2	166	24	0.07	0.08	1.23	0.02	0.04	2.23	100

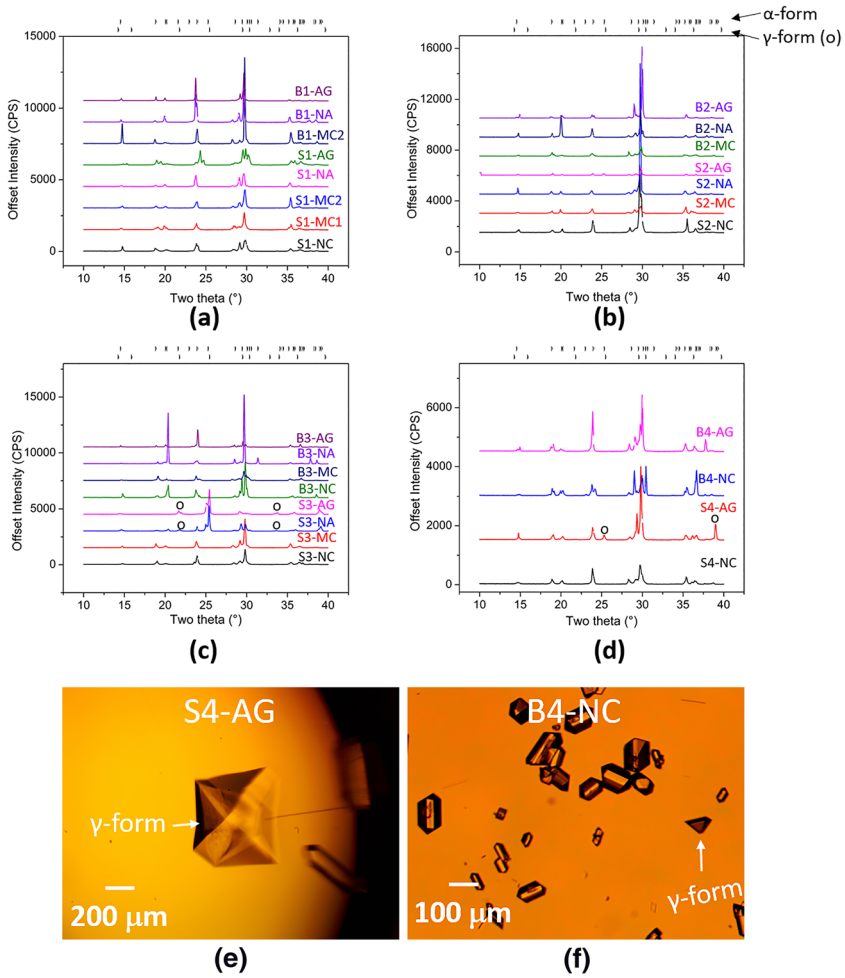

Fig. 3 **a**–**d** XRD spectra of dried product crystals at starting concentration of **a** 0.30, **b** 0.32, **c** 0.34, and **d** 0.36 g/g water. The characteristic peaks for γ-form crystals [40, 44–46] are circled on the XRD spectra. **e**, **f** Representative microscopy images of glycine product slurry containing γ-form crystals directly from **e** slug-flow crystallizer and **f** batch crystallizer. (The γ-form crystals are pointed by arrows, based on comparison with typical images in literature [41], among α-form crystals without arrows.)

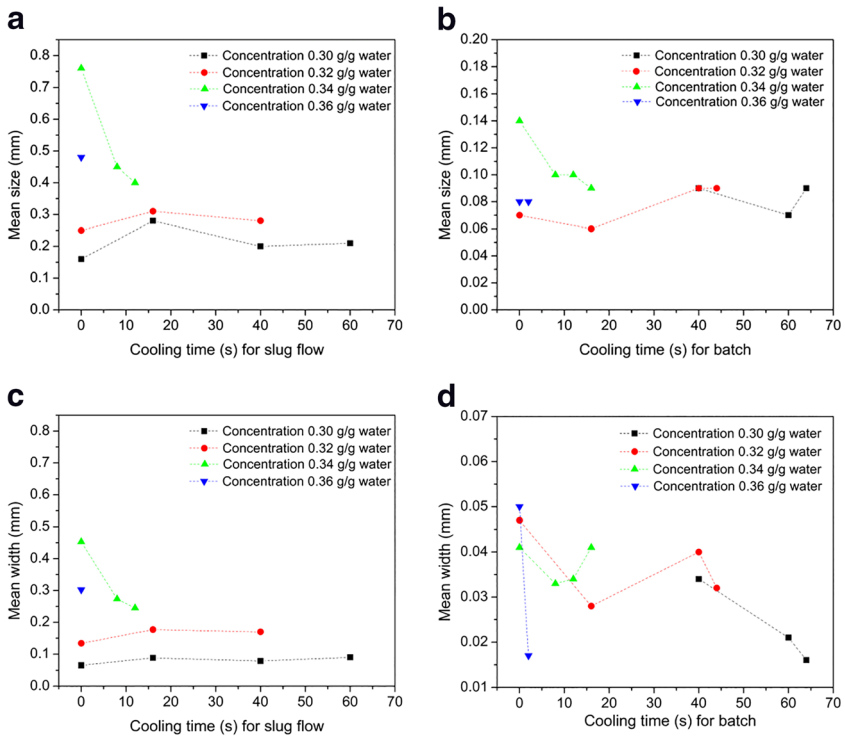

Fig. 4 **a**, **b** Mean length ("size") of product crystals from **a** slug flow and **b** batch crystallization at different starting concentrations and cooling time. Each experiment in Table 1 is one data point on the plot. (B1-NC and B1-MC1 did not nucleate; hence, no data showed.) The same concentration data are connected with dashed color lines of different colors. **c**, **d** Mean width of product crystals from **c** slug flow and **d** batch crystallization experiments at conditions in **a** and **b**. Besides the size mean, other size statistics (e.g., standard deviation and coefficient of variation) of product crystals are included in Tables 2 and 3, respectively

(slope in the temperature-time profile in Fig. 1c and d) thus larger maximum supersaturation and higher nucleation rate [4].

Upper Bound of Crash Cooling Time for Pure α-Form Without Aggregation

Crash cooling time was defined as the contact time of the solution and cold surface at 4 °C (in ice bags). In slug flow with an average flow rate of 25 mm/s, the cooling time for each slug is translated into cooling zone length as in Table 1. As the cooling temperature (4 °C) is much lower than the end temperature, increasing cooling time is expected to facilitate crystallization (details in the "Lower Bound of Crash Cooling Time: Natural Cooling" section comparing natural cooling and crash cooling). For the same starting and ending conditions (concentration, temperature), the longer the *crash cooling time*, the longer the residence time at high and/or maximum supersaturation, thus the larger portion of slugs nucleated (Table 2). Longer cooling time is required for lower starting concentration to increase the portion of nucleated slugs close to 100% (Table 2). For example, at concentration of 0.30 g/g water, the portion of nucleated slugs is 92% under 1.5 m cooling length. When the starting concentration increased to 0.34 g/g water, 0.3 m cooling length will lead to 96% of nucleated slugs.

There exists an "upper bound" for crash cooling time without aggregation, beyond which "flower"-shaped crystal aggregations (Fig. S4) appear. The transition of aggregation situation only occurs within a small change of cooling time, such as a few seconds (Fig. 2). Compared with corresponding slug flow, the excess cooling time induced aggregation for slug flow did not cause aggregation in the batch crystallization process. It is reasonable because the batch crystallization has smaller maximum supersaturation in practice (Fig. 1c, d), due to the smaller heat release rate. Figure 2 also indicates that this upper limit (referred to as "maximum cooling time without aggregation") is directly affected by the starting concentration. The higher the concentration, the smaller the maximum time, and the narrower the cooling time range without aggregation.

The green dots in Fig. 5 indicate pure α-form and non-aggregating crystals. These crystals were analyzed earlier (e.g., Figs. 2 and 4, Table 2) to be in narrow size distribution as well; thus, the "green zone" (composed of green dots) can be viewed as the feasible operational zone for slug-flow cooling crystallization of glycine. Red dots in Fig. 5 indicate the existence of either aggregation (among non-aggregation populations) or form (among majority α-forms). Note that aggregation does not always come with a different crystal form. For example, at low starting concentration (0.30 and 0.32 g/g water), all product crystals from batches and SFCs are α-form, even when crystals aggregate (the longest cooling time in Fig. 5a). When the starting concentration increases to 0.34 g/g water, γ-form appears at short crash cooling times, before crystals start to aggregate (condition S3-NA in Fig. 1b).

Beyond Upper Bounds: γ-Form Glycine Crystals Generated from Cooling Aqueous Slugs

At a starting concentration of 0.30 and 0.32 g/g water, with either zero or maximum crash cooling time (for aggregation), the glycine crystals generated from SFC or batch crystallizers are 100% in the α-form (Fig. 3a, b). When the starting concentration increases from 0.32 g/g (increased supersaturation, Fig. 1c, d), natural cooling still produces crystals 100% in the α-form, but maximum cooling or longer time produces some γ-form crystals among α-forms (Fig. 3, Tables 2 and 3). The existence of γ-form under certain crystallization conditions was confirmed using powder XRD, and a few γ-form crystals were also identified in some microscope images of the slurry (Fig. 3e, f) immediately/directly from both slug flow and batch crystallization, based on comparison with images of γ-form crystals in literature [41]. The higher supersaturation likely facilitates the overcoming of the energy barrier to nucleation and grows γ-form crystals [33, 54], besides the common metastable α-form.

All conditions here generate mostly (if not all) α-form crystals, which is expected with literature [40–42, 55, 56] and in commercial glycine (used as starting materials) [32] (Fig. 1e, f). No β-form was observed, based on neither XRD nor microscope images, even though β-form may be generated together with α-form from pure aqueous solution (e.g., through cooling) [41, 55]. The no-appearance of β-form is likely due to its instability [41] and possible transition to α- or γ-forms [45, 50]. The generation of γ-form glycine after 10 min without the addition of additives (by using cooling only) can be interesting. From literature, the γ-form glycine crystals (trigonal-hexagonal structure) are usually generated from water by evaporation [40, 56] or adding additives, such as salt [41, 42] and acid [55]. Recent discoveries showed that certain concentration ranges (e.g., 0.4–0.525 g/g water) [33, 54] and/or at range (~0.3–0.35 g/g water) with residence time up to 1 h [37] may help induce the generation of γ-form among α-form (majority), without additives. And, our study not only agrees with the existing studies but also shows that the γ-form can be formed at a lower concentration (e.g., 0.36–0.38 g/g water) or shorter time (e.g., 10 min), if in slug flow. The larger characteristic peaks of γ-form for slug flow than batches (Fig. 3c, d) also indicate a higher portion of γ-form glycine crystals in the slug-flow process.

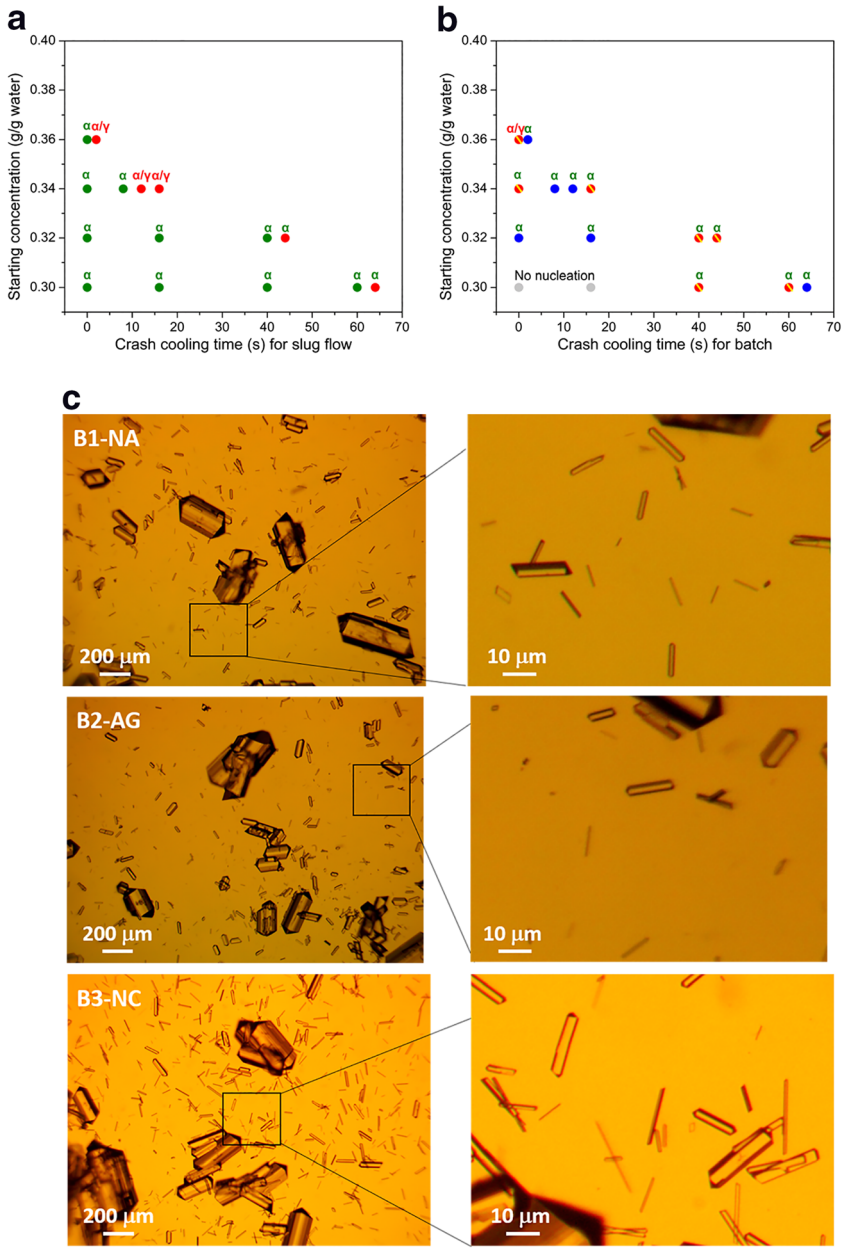

Fig. 5 **a** Diagram of product crystal quality (polymorphic form, aggregation situation, and needle-shaped existence) from **a** slug-flow crystallization and **b** corresponding batch crystallization. Their experimental conditions are detailed in Table 1, such as the starting solution concentration and crash cooling time. Green dots are for non-aggregating α-form with narrow size distribution (including natural cooling), and red dots for aggregation and/or γ-form. The yellow line inside the dots indicates the presence of needle-shaped crystals. Aggregations (for slug-flow products) are indicated with "-AG" in the condition label of Fig. 1b and Tables 1, 2, and 3, with microscope images in Fig. S4. Needle-shaped crystals are indicated with red dots with a backward yellow slash symbol. **c** Representative microscopy images zoomed in for product crystals from batch, indicating the existence of needle-shaped crystals. With the same zoom in double check, there are no tiny crystals observed from slug-flow results in Fig. 2

Conclusion

Non-aggregating α-form glycine crystals were continuously generated after 10 min, from cooling solution in slug flow, without using pre-made seeds nor additives such as antisolvent. The crystal quality (form purity, narrow size distribution, and non-aggregation) can be maintained for multiple operational conditions (combinations of crash cooling time and starting concentration) at the same fast production rate. The higher the cooling time and starting concentration, the higher the probability of primary nucleation, and the lower the maximum cooling time without aggregation. When the cooling time further increases beyond the maximum time, some "flower-shaped" crystal aggregations and γ-form crystals appear. At proper starting concentrations, natural cooling was also shown to be able to nucleate and grow non-aggregated α-form crystals in slug flow. Most cooling crystallization conditions carried out in slug flow generally lead to more uniform and larger crystals (and minimizes needle-shaped crystals) than in corresponding batches. At low starting concentrations and/or cooling time, slug flow can nucleate crystals when batches fail to nucleate. In the future, the molecular mechanism for these interesting phenomena will be explored.

Acknowledgments Virginia Commonwealth University is acknowledged for the financial support.

Compliance with Ethical Standards

Conflict of Interest The authors declare that they have no conflict of interest.

References

1. Myerson AS. Handbook of industrial crystallization. 2nd ed. Woburn, MA: Butterworth-Heinemann; 2002.
2. Mullin JW. Crystallization. 4th ed. Oxford: Butterworth-Heinemann; 2001.
3. Tung H-H, Paul EL, Midler M, McCauley JA. Crystallization of pharmaceuticals: an industrial perspective. Hoboken, NJ: Wiley; 2009.
4. Lewis EA, Seckler MM, Kramer H, van Rosmalen G. Industrial crystallization: fundamentals and applications. Cambridge: Cambridge University Press; 2015.
5. Yu LX. Pharmaceutical quality by design: product and process development, understanding, and control. Pharm Res. 2008;25:781–91.
6. Zhang D, Xu S, Du S, Wang J, Gong J. Progress of pharmaceutical continuous crystallization. Engineering. 2017;3:354–64.
7. Rimez B, Debuysschère R, Conté J, Lecomte-Norrant E, Gourdon C, Cognet P, et al. Continuous-flow tubular crystallization to discriminate between two competing crystal polymorphs. 1. Cooling crystallization. Cryst Growth Des. 2018;18:6431–9.
8. Narayan ST. Industrial crystallization: process simulation analysis and design. Boston, MA: Springer; 1995.
9. Wang H, Mustaffar A, Phan AN, Zivkovic V, Reay D, Law R, et al. A review of process intensification applied to solids handling. Chem Eng Process Process Intensif. 2017;118:78–107.
10. Nagy ZK, Fujiwara M, Braatz RD. Monitoring and advanced control of crystallization processes. In: Lee AY, Myerson AS, Erdemir D, editors. Handb. Ind. Cryst. 3rd ed. Cambridge: Cambridge University Press; 2019.
11. Lovette MA, Browning AR, Griffin DW, Sizemore JP, Snyder RC, Doherty MF. Crystal shape engineering. Ind Eng Chem Res. 2008;47:9812–33.
12. Brown CJ, McGlone T, Yerdelen S, Srirambhatla V, Mabbott F, Gurung R, et al. Enabling precision manufacturing of active pharmaceutical ingredients: workflow for seeded cooling continuous crystallisations. Mol Syst Des Eng. 2018;3:518–49.
13. Wang T, Lu H, Wang J, Xiao Y, Zhou Y, Bao Y, et al. Recent progress of continuous crystallization. J Ind Eng Chem. 2017;54:14–29.
14. Jiang M, Braatz RD. Designs of continuous-flow pharmaceutical crystallizers: developments and practice. CrystEngComm. 2019;21:3534–51.
15. Lawton S, Steele G, Shering P, Zhao L, Laird I, Ni XW. Continuous crystallization of pharmaceuticals using a continuous oscillatory baffled crystallizer. Org Process Res Dev. 2009;13:1357–63.
16. Power G, Hou G, Kamaraju VK, Morris G, Zhao Y, Glennon B. Design and optimization of a multistage continuous cooling mixed suspension, mixed product removal crystallizer. Chem Eng Sci. 2015;133:125–39.
17. Li J, Trout BL, Myerson AS. Multistage continuous mixed-suspension, mixed-product removal (MSMPR) crystallization with solids recycle. Org Process Res Dev. 2016;20:510–6.
18. Briggs NEB, Schacht U, Raval V, McGlone T, Sefcik J, Florence AJ. Seeded crystallization of β-L-glutamic acid in a continuous oscillatory baffled crystallizer. Org Process Res Dev. 2015;19:1903–11.
19. Jiang M, Li Y-EED, Tung H-HH, Braatz RD. Effect of jet velocity on crystal size distribution from antisolvent and cooling crystallizations in a dual impinging jet mixer. Chem Eng Process Process Intensif Elsevier BV. 2015;97:242–7.
20. Alvarez AJ, Myerson AS. Continuous plug flow crystallization of pharmaceutical compounds. Cryst Growth Des. 2010;10:2219–28.
21. Hohmann L, Greinert T, Mierka O, Turek S, Schembecker G, Bayraktar E, et al. Analysis of crystal size dispersion effects in a continuous coiled tubular crystallizer: experiments and modeling. Cryst Growth Des. 2018;18:1459–73.
22. Eder RJP, Radl S, Schmitt E, Innerhofer S, Maier M, Gruber-Woelfler H, et al. Continuously seeded, continuously operated tubular crystallizer for the production of active pharmaceutical ingredients. Cryst Growth Des. 2010;10:2247–57.
23. Wiedmeyer V, Anker F, Bartsch C, Voigt A, John V, Sundmacher K. Continuous crystallization in a helically coiled flow tube: analysis of flow field, residence time behavior, and crystal growth. Ind Eng Chem Res. 2017;56:3699–712.
24. Han B, Ezeanowi NC, Koiranen TO, Häkkinen AT, Louhi-Kultanen M. Insights into design criteria for a continuous, sonicated modular tubular cooling crystallizer. Cryst Growth Des. 2018;18:7286–95.
25. Mou M, Li H, Yang B-S, Jiang M. Continuous generation of millimeter-sized glycine crystals in non-seeded millifluidic slug flow. Crystals. 2019;9:412.
26. Robertson K, Flandrin P-B, Klapwijk AR, Wilson CC. Design and evaluation of a mesoscale segmented flow reactor (KRAIC). Cryst Growth Des. 2016;16:4759–64.
27. Jiang M, Papageorgiou CD, Waetzig J, Hardy A, Langston M, Braatz RD. Indirect ultrasonication in continuous slug-flow crystallization. Cryst Growth Des. 2015;15:2486–92.
28. Jiang M, Zhu Z, Jimenez E, Papageorgiou CD, Waetzig J, Hardy A, et al. Continuous-flow tubular crystallization in slugs spontaneously induced by hydrodynamics. Cryst Growth Des. 2014;14:851–60.
29. Besenhard MO, Hohl R, Hodzic A, Eder RJP, Khinast JG. Modeling a seeded continuous crystallizer for the production of active pharmaceutical ingredients. Cryst Res Technol. 2014;49:92–108.
30. Rasche ML, Jiang M, Braatz RD. Mathematical modeling and optimal design of multi-stage slug-flow crystallization. Comput Chem Eng. 2016;95:240–8.
31. Besenhard MO, Neugebauer P, Scheibelhofer O, Khinast JG. Crystal engineering in continuous plug-flow crystallizers. Cryst Growth Des. 2017;17:6432–44.
32. Su M, Gao Y. Air-liquid segmented continuous crystallization process optimization of the flow field, growth rate, and size distribution of crystals. Ind Eng Chem Res. 2018;57:3781–91.
33. Rabesiaka M, Sghaier M, Fraisse B, Porte C, Havet JL, Dichi E. Preparation of glycine polymorphs crystallized in water and physicochemical characterizations. J Cryst Growth [Internet]. Elsevier; 2010;312:1860–1865. Available from: https://doi.org/10.1016/j.jcrysgro.2010.03.011
34. Hamilton BD, Hillmyer MA, Ward MD. Glycine polymorphism in nanoscale crystallization chambers. Cryst Growth Des. 2008;8:3368–75.
35. Bonnin-Paris J, Stéphane B, Jean-Louis H, Fauduet H. Determination of the metastable zone width of Glycine aqueous solutions for batch crystallizations. Chem Eng Commun. 2011;198:1004–17.
36. Moscosa-Santillán M, Bals O, Fauduet H, Porte C, Delacroix A. Study of batch crystallization and determination of an alternative temperature-time profile by on-line turbidity analysis-application to glycine crystallization. Chem Eng Sci. 2000;55:3759–70.
37. Little LJ, Sear RP, Keddie JL. Does the γ polymorph of glycine nucleate faster? A quantitative study of nucleation from aqueous solution. Cryst Growth Des. 2015;15:5345–54.

38. Dandekar P, Kuvadia ZB, Doherty MF. Engineering crystal morphology. Annu Rev Mater Res. 2013;43:359–86.
39. Renuka Devi K, Gnanakamatchi V, Srinivasan K. Attainment of unstable β nucleation of glycine through novel swift cooling crystallization process. J Cryst Growth [Internet]. 2014;400:34–42. Elsevier; Available from:. https://doi.org/10.1016/j.jcrysgro.2014.04.029.
40. He G, Bhamidi V, Wilson SR, Tan RBH, Kenis PJA, Zukoski CF. Direct growth of γ-glycine from neutral aqueous solutions by slow, evaporation-driven crystallization. Cryst Growth Des. 2006;6:1746–9.
41. Srinivasan K. Crystal growth of α and γ glycine polymorphs and their polymorphic phase transformations. J Cryst Growth. 2008;311:156–62.
42. Bhat MN, Dharmaprakash SM. Effect of solvents on the growth morphology and physical characteristics of nonlinear optical γ-glycine crystals. J Cryst Growth. 2002;242:245–52.
43. Neugebauer P, Cardona J, Besenhard MO, Peter A, Gruber-Woelfler H, Tachtatzis C, et al. Crystal shape modification via cycles of growth and dissolution in a tubular crystallizer. Cryst Growth Des. 2018;18:4403–15.
44. Kudo S, Takiyama H. Production of fine organic crystalline particles by using milli segmented flow crystallizer. J Chem Eng Jpn. 2012;45:305–9.
45. Perlovich GL, Hansen LK, Bauer-Brandl A. The polymorphism of glycine: thermochemical and structural aspects. J Therm Anal Calorim. 2001;66:699–715.
46. Netzel J, Hofmann A, Van Smaalen S. Accurate charge density of α-glycine by the maximum entropy method. CrystEngComm. 2008;10:335–43.
47. Langan P, Mason SA, Myles D, Schoenborn BP. Structural characterization of crystals of α-glycine during anomalous electrical behaviour. Acta Crystallogr Sect B Struct Sci International Union of Crystallography. 2002;58:728–33.
48. Barrett P, Smith B, Worlitschek J, Bracken V, O'Sullivan B, O'Grady D. A review of the use of process analytical technology for the understanding and optimization of production batch crystallization processes. Org Process Res Dev. 2005;9:348–55.
49. Chen J, Sarma B, Evans JMBB, Myerson AS. Pharmaceutical crystallization. Cryst Growth Des American Chemical Society. 2011;11:887–95.
50. Jiang Q, Shtukenberg AG, Ward MD, Hu C. Non-topotactic phase transformations in single crystals of β-glycine. Cryst Growth Des. 2015;15:2568–73.
51. Daniel Scott C, Labes R, Depardieu M, Battilocchio C, Davidson MG, Ley SV, et al. Integrated plug flow synthesis and crystallisation of pyrazinamide. React Chem Eng. 2018;3:631–4.
52. Majumder A, Nagy ZK. Fines removal in a continuous plug flow crystallizer by optimal spatial temperature profiles with controlled dissolution. AICHE J. 2013;59:4582–94.
53. Giulietti M, Seckler MM, Derenzo S, Ré MI, Cekinski E. Industrial crystallization and precipitation from solutions: state of the technique. Brazilian J Chem Eng SCIELO. 2001;18:423–40.
54. Vesga MJ, McKechnie D, Mulheran PA, Johnston K, Sefcik J. Conundrum of γ glycine nucleation revisited: to stir or not to stir? CrystEngComm Royal Society of Chemistry. 2019;21:2234–43.
55. Anbu Chudar Azhagan S, Kathiravan VS, Sathiya Priya N. Crystallization, habit modification and control of nucleation of glycine polymorphs from aqueous solutions doped with magnesium sulfate impurity. Mater Sci Pol. 2018;36:483–93.
56. Di Profio G, Tucci S, Curcio E, Drioli E. Selective glycine polymorph crystallization by using microporous membranes. Cryst Growth Des. 2007;7:526–30.